NUCET NUCLEAR ENERGY AND TECHNOLOGY

Nuclear Energy and Technology 12(2): 77–83
DOI 10.3897/nucet.12.196493

Research Article

Direct numerical simulation of 2D and 3D bubble rise in liquid metal coolant

Vladimir V. Chudanov[1], Anna E. Aksenova[1], Mikhail V. Bayaskhalanov[2], Alexey A. Leonov[1,2], Artem A. Makarevich[1]

1 *Nuclear Safety Institute of the Russian Academy of Sciences (IBRAE RAN), Moscow, Russia*

2 *National Research Nuclear University MEPhI (Moscow Engineering Physics Institute), Moscow, Russia*

Corresponding author: Mikhail V. Bayaskhalanov (mvbayaskhalanov@mephi.ru)

Academic editor: Anton Smirnov ♦ **Received** 27 April 2026 ♦ **Accepted** 28 May 2026 ♦ **Published** 3 June 2026

Citation: Chudanov VV, Aksenova AE, Bayaskhalanov MV, Leonov AA, Makarevich AA (2026) Direct numerical simulation of 2D and 3D bubble rise in liquid metal coolant. Nuclear Energy and Technology 12(2): 77–83. https://doi.org/10.3897/nucet.12.196493

Abstract

A numerical model for direct numerical simulation of compressible two-phase media is applied to the problem of gas-bubble rise in liquid lead. Because liquid metals are opaque and exhibit a very large density contrast between the gas and liquid phases, direct numerical simulation is an important tool for investigating interfacial dynamics and bubble-shape evolution. The paper presents 2D and 3D calculations performed with a two-phase flow code under development at IBRAE RAN using a previously developed surface-tension model integrated into the numerical algorithm. The numerical algorithm employs an explicit HLLC scheme with MUSCL reconstruction and equations of state to model compressible two-component media. The code is designed for the direct numerical simulation of thermal fluid dynamics in a two-phase compressible medium, including two-component mixtures, accounting for interfacial heat and mass transfer and using equations of state for Stiffened Gas or the Noble-Abel equation for weakly compressible media. The computed evolution of bubble shape and the time-dependent rise velocity are compared against experimental data for bubble rise in narrow rectangular channels. The simulated value of the rise velocity of a gas bubble with initial diameter of 3 mm agrees with the experimental average value of the rise velocity of moderate bubbles, entering the experimental channel through a nozzle of 3 mm in size, within 40%. This discrepancy is attributed to the insufficiently fine computational mesh used in the simulations.

Keywords

direct numerical simulation; two-phase flow; liquid lead; bubble rise; surface tension; heavy liquid-metal coolant

Introduction

For flow conditions in the circulation loops of reactor systems employing heavy liquid-metal coolants, the simulation of two-phase flows involving liquid lead and a gas phase is of considerable practical importance. The relevance of such studies is confirmed by Khomyakov et al. (2023), who examined the potential hazards associated with steam-generator leakage in a lead-cooled reactor. Because this coolant is much denser than water, the gas-to-liquid density ratio is far smaller than in a water-gas system. The large density contrast increases the buoyancy of the gas phase and strongly affects the shape, size, and evolution of gas bubbles in liquid metal. Among the studies devoted to such flows, the review by Xiuzhong and Takashi (2021) is particularly noteworthy: it summarizes experiments on the rise-velocity distribution of gas inclusions in upward gas-liquid-metal two-phase flow for

Copyright *Chudanov VV et al.* This is an open access article distributed under the terms of the Creative Commons Attribution License (CC-BY 4.0), which permits unrestricted use, distribution, and reproduction in any medium, provided the original author and source are credited.

channels of different geometries, reviews existing models, and compares them with experimental data obtained in circular pipes, rectangular channels, and narrow gaps. That comparison showed that none of the available models describes the experimental data with sufficient accuracy. Kuzina and Sorokin (2024) also identified, among the current challenges in modeling thermal-hydraulic processes in liquid-metal-cooled reactors, the need to improve methods for predicting local turbulent characteristics of momentum and energy transport in two-phase flows. Direct visual observation of two-phase flow in liquid metal is severely limited by its complete opacity. Under these conditions, direct numerical simulation using dedicated two-phase flow codes becomes an essential tool.

In high-fidelity calculations of two-phase-flow evolution, surface-tension modeling is a key component of the numerical algorithm. This paper presents the results of model calculations for a gas bubble rising in liquid lead using a previously developed surface-tension methodology integrated into the numerical algorithm of a two-phase flow code currently under development at IBRAE RAN. The code is intended for direct numerical simulation of thermal fluid dynamics in a compressible two-phase medium, including two-component mixtures, with allowance for interfacial heat and mass transfer and with equations of state for stiffened gas or Noble-Abel media in the weakly compressible media. The code is intended for simulations of single-phase and two-phase flows in reactor components and experimental facilities with gas, water, or liquid-metal coolants, including pipelines, individual rods, and large coolant-filled volumes.

Methods

Two-Phase Flow Model

To calculate the evolution of the two-phase medium, the code employs a six-equation model (Saurel et al. 2009) supplemented by terms accounting for viscosity, surface tension, and gravity. Heat and mass transfer are neglected in the calculations presented here; accordingly, the governing equations of the model can be written in the form given by Berry et al. (2008):

$$\begin{cases} \frac{\partial \alpha_g}{\partial t} + \vec{u}\vec{\nabla}\alpha_g = \mu\,(p_g - p_l) \\ \frac{\partial \rho}{\partial t} + \mathrm{div}(\rho\vec{u}) = 0 \\ \frac{\partial \rho Y_l}{\partial t} + \mathrm{div}\left(\rho Y_l \vec{u}\right) = 0 \\ \frac{\partial \rho\vec{u}}{\partial t} + \overrightarrow{\mathrm{div}}\left(\rho\vec{u}\otimes\vec{u} + P\bar{\bar{I}} - \sigma\left(|\boldsymbol{w}|\bar{\bar{I}} - \frac{\boldsymbol{w}\otimes\boldsymbol{w}}{|\boldsymbol{w}|}\right) - v\bar{\bar{\tau}}\right) = \rho\vec{g} \\ \frac{\partial \alpha_g\rho_g e_g}{\partial t} + \mathrm{div}\left(\alpha_g\rho_g e_g\vec{u} - \alpha_g v_g\bar{\bar{\tau}}_g\right) - \alpha_g p_g\,\mathrm{div}\,\vec{u} = -p_I\mu\,(p_g - p_l) + \alpha_g\rho_g\vec{u}\vec{g} \\ \frac{\partial \alpha_l\rho_l e_l}{\partial t} + \mathrm{div}\left(\alpha_l\rho_l e_l\vec{u} - \alpha_l v_l\bar{\bar{\tau}}_l\right) - \alpha_l p_l\,\mathrm{div}\,\vec{u} = p_I\mu\,(p_g - p_l) + \alpha_l\rho_l\vec{u}\vec{g} \end{cases} \quad (1)$$

where, α_k, ρ_k, p_k, e_k are the volume fraction, density, pressure, and specific internal energy of phase k ($k = g$ – is the gas phase, $k = l$ is the liquid phase); $\rho = \alpha_g\rho_g + \alpha_l\rho_l$, $P = \alpha_g\rho_g + \alpha_l\rho_l$, $Y_l = \alpha_l\rho_l/\rho$); are the density and pressure of the two-phase media and the mass fraction of the liquid phase, respectively; $\rho_l =$ is the interfacial pressure from Saurel et al. (2009); c_k is the speed of sound in phase k ($k = g, l$); $w = \nabla\alpha$; σ is the surface-tension coefficient; μ is the pressure-relaxation coefficient; v_k is the dynamic viscosity of phase k ($k = g, l$); $v = \alpha_g v_g + \alpha_l v_l$ is the dynamic viscosity of the two-phase media; $\bar{\bar{\tau}}$ is the viscous stress tensor; and $\vec{g}$ is the gravitational acceleration.

The methodology used to calculate the components of vector w associated with surface tension is described by Chudanov et al. (2025). System (1) is solved numerically using an explicit scheme with an HLLC (Harten-Lax-van Leer-Contact) solver (Toro 2019), adapted for two-phase media and for the stiffened-gas (Le Metayer et al. 2004) or Noble-Abel (Le Metayer and Saurel, 2016) equations of state used as closure relations. In addition, the numerical solution of a redundant conservative equation for the total energy of the two-phase mixture is used to compute the pressure-correction term (Saurel et al. 2009). The explicit formulation provides near-ideal scalability when parallel computing technologies are used. Second-order accuracy in space and time is achieved by the MUSCL Monotonic Upstream-centered Scheme for Conservation Laws) algorithm, which uses directional differences in the grid approximation of thermodynamic-variable profiles. The algorithm implements a two-step predictor-corrector procedure together with operator splitting by physical process. During the predictor step, the part of the system describing gas-dynamic processes and the influence of surface tension is solved. The viscous terms are treated as corrections to the solution and are incorporated at the corrector step.

The proposed methodology was validated against an analytical benchmark reported in the literature (Lebaigue et al. 2004): the rise of a spherical bubble in a quiescent liquid. To assess the capability of the numerical scheme to reproduce surface-tension effects, 2D and 3D simulations of a gas bubble rising in liquid lead were then performed. The computed rise velocity was compared with the experimental rise velocity of small bubbles obtained by Pribaturin et al. (2024).

Methodology Testing on an Analytical Benchmark

The benchmark problem of a spherical bubble rising in a liquid initially at rest is informative because it provides not only the final bubble shape, which is a practical comparison criterion, but also the full time history of the

bubble velocity, from rest through the overshoot to the asymptotic terminal value. To reproduce the correct terminal velocity and the velocity overshoot, the numerical method must accurately account for buoyancy, viscous stresses, and surface tension. In particular, this test allows for the verification of the numerical model regarding the transition conditions at the interface.

A liquid inclusion rising in another liquid is considered. Both the inclusion and the surrounding liquid are initially at rest. Gravitational buoyancy is the only driving force. The test consists in computing the transient acceleration of the rising inclusion until a constant terminal velocity is reached.

The physical model reduces to the Navier-Stokes equations in both phases with constant surface tension at the interface. No phase change occurs at the interface. Because the solution does not depend on whether one or both phases are weakly compressible, the benchmark can be considered in either compressible or incompressible form, depending on the numerical method under evaluation.

Reference solutions are available in dimensionless form, however, a representative set of dimensional physical parameters is also proposed. The characteristic length scale of the problem is the initial inclusion diameter d_e. The characteristic velocity scale for the center-of-mass velocity U is:

$$U_c = \sqrt{g d_e}, \tag{2}$$

where g is the acceleration of gravity. The time scale is:

$$t_c = \sqrt{d_e / g} \tag{3}.$$

The reduced parameters are $\tau = t/t_c$ and $u = U/U_c$. According to these definitions, the evolution of the center-of-mass displacement velocity in dimensionless form is defined by the expression:

$$u = U/U_c = f(\tau) = f\,(t/t_c) \tag{4}.$$

The calculation may be performed either in an axisymmetric domain or in the original three-dimensional domain. Because the finite extent of the computational domain affects the terminal velocity of the inclusion, the domain size must be increased until its influence on the result becomes negligible. As a first estimate, the domain is assumed to extend by at least ten diameters in all directions.

According to Blanco-Alvarez (1995), the shape itself does not determine the required domain expansion, whereas the modification of the terminal bubble growth rate can be estimated using the following semi-empirical relation:

$$\frac{U_c^{\text{confined}}}{U_c^{\infty}} \approx 1 - \left(\frac{d_e}{D}\right)^2 \tag{5}$$

where D is the characteristic size of the domain in the plane perpendicular to the direction of gravity.

The physical parameters, namely ρ_L and ρ_V (the densities of the surrounding liquid and the liquid inclusion, respectively), μ_L and μ_v (the dynamic viscosities), σ (the surface tension) are selected so as to reproduce the appropriate values of the dimensionless quantities for which reference calculations are available: the Morton number Mo, the Bond number Bo, and density ρ_L/ρ_V and viscosity μ_L/μ_V ratios.

The Morton and Bond numbers are defined as

$$\text{Mo} = \frac{g\mu_L^4}{\rho_L \sigma^3} \tag{6},$$

and

$$\text{Bo} = \frac{\rho_L g d_\varepsilon^2}{\sigma} \tag{7}.$$

The displacement of a liquid inclusion with the following dimensionless properties must be computed:

Mo = 0.056, Bo = 40, $\rho_L / \rho_v = 100$ and $\mu_L / \mu_v = 100$.

As an example, the following physical properties are proposed:

$\rho_L = 1000$ kg/m^3, $\rho_V = 10$ kg/m^3,

$\mu_L = 0.273556$ Pa/s and $\mu_v = 0.00273556$ Pa/s,

$\sigma = 0.1$ N/m, $g = 10$ m/s^2, $d_e = 0.02$ m.

The position of the inclusion center of mass is extracted, after which the translational velocity is determined. The first comparison criterion is the reduced asymptotic velocity. Naturally, in this case, the time evolution of the overshoot point (Fig. 1) cannot be fixed. In addition to the main result, the dimensionless overshoot during the velocity rise can also be compared. Fig. 2 compares the numerical predictions with the reference data for bubble growth rate as a function of time. As can be seen, the agreement is good both in the dynamics and in the overall shape of the velocity curve. Fig. 3 shows the calculated flow patterns for a single rising bubble in both 2D (a) and 3D (b).

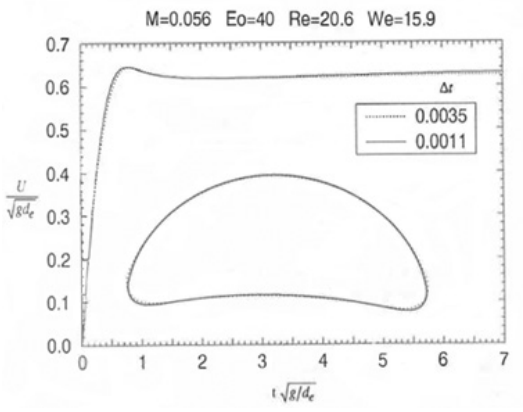

Figure 1. Reduced time evolution of displacement velocity for two grid sizes, adapted from Lebaigue et al. (2004)

The differences between bubble rise in two-dimensional and three-dimensional simulations are associated with fundamental differences in flow topology, hydrodynamic resistance, and pressure distribution. In a three-dimensional domain, the surrounding liquid can flow around the

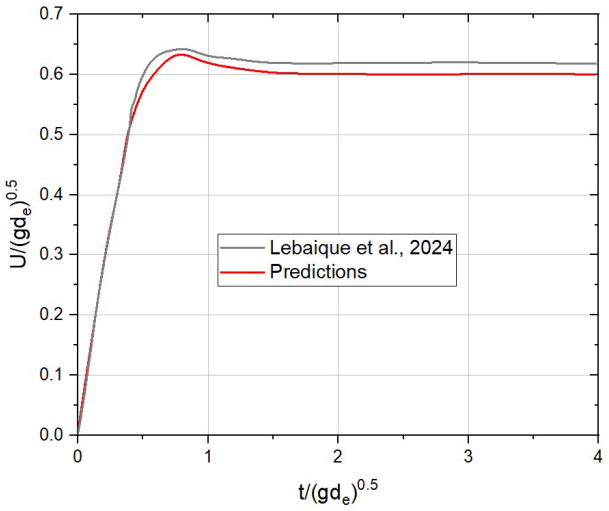

Figure 2. Bubble growth rate as a function of time: numerical predictions compared with the reference data reported by Lebaigue et al. (2004)

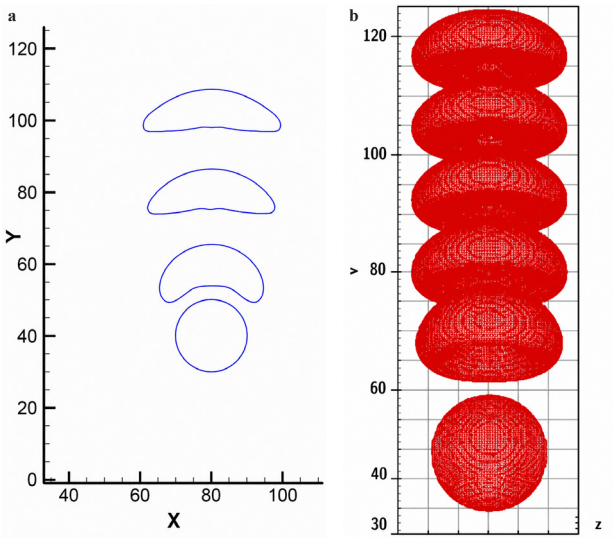

Figure 3. Calculated flow patterns for a single rising bubble: 2D (**a**) and 3D (**b**).

bubble in all directions, whereas the planar formulation imposes additional kinematic constraints. The higher peak and terminal velocities observed in the three-dimensional simulations can be attributed primarily to reduced hydrodynamic drag, more realistic buoyancy-driven deformation, and fully three-dimensional displacement of the surrounding liquid. In the two-dimensional formulation, a region of low pressure and strong vortical structures forms behind the bubble, increasing drag and slowing the rise. In a three-dimensional flow, the liquid can bypass the bubble more freely, which reduces the effective drag force. The planar constraint also affects bubble deformation. Since the motion of the fluid is restricted in the out-of-plane direction, the bubble shape may deviate from physically realistic three-dimensional configurations. This artificial deformation influences the balance between buoyancy, inertia, viscous stresses, and surface tension. Finally, buoyancy and surface-tension forces scale differently with bubble geometry. Buoyancy is associated with displaced volume, whereas surface tension is associated with interfacial area. Therefore, a three-dimensional bubble can adopt a more physically realistic and energetically favorable shape, such as a spherical or ellipsoidal configuration, which promotes faster upward motion.

Previous hydrodynamic studies have shown that two-dimensional bubble simulations are strongly affected by artificial confinement and boundary effects. The present three-dimensional results confirm that geometric freedom in the out-of-plane direction can significantly increase the bubble rise velocity, in this case by more than 50%.

Results and discussion

2D Simulation of Gas-Bubble Rise in Liquid Lead

2D simulation of gas-bubble rise in liquid lead. The computational domain is a rectangular channel measuring 15 × 30 mm² in the XY plane. The channel is filled with liquid lead with a density of 10^4 kg/m³ and is placed in a gravitational field (g = –9.81 m/s²). At the initial time, a circular gas bubble of radius 1.5 mm and density 1 kg/m³ is located in the lower part of the channel (X_0 = 7.5 mm; Y_0 = 5 mm). Under the action of buoyancy, the light gas bubble rises upward. Reflection and slip boundary conditions are imposed on the lateral and lower boundaries of the computational domain. The upper boundary is treated as a free surface. At the initial time, the pressure in the uppermost horizontal cross-section is equal to atmospheric pressure; downward in the vertical direction, the pressure increases under the action of gravity. The stiffened-gas equation of state is used for both lead and gas, with coefficient values listed in Table 1. The surface-tension coefficient of lead was taken to be 0.4 N/m. The dynamic viscosity was set to 0.002 Pa·s. The calculation was performed on a 128 × 256 cell grid using an explicit second-order scheme in both space and time. A combined 0,5×minmod+0,5×superbee limiter was used to compute limited slopes of the thermodynamic-variable profiles. The time step was determined from the Courant number condition *courant* = 0.2.

Table 1. Used values of coefficients for the Stiffened Gas equation of state

Coefficient	Gas	Lead
C_v, j/kg × K	1040	1816
C_p, j/kg × K	1456	3814
γ	1.4	2.1
π, Pa	0	8.45×10^9

Fig. 4 shows the 2D results in terms of the contour enclosing the region where the gas volume fraction exceeds 0.5 at the following time instants: 0 (a), 23.3 (b), 47.3 (c), 77.9 (d), 115 (e), and 194 ms (f).

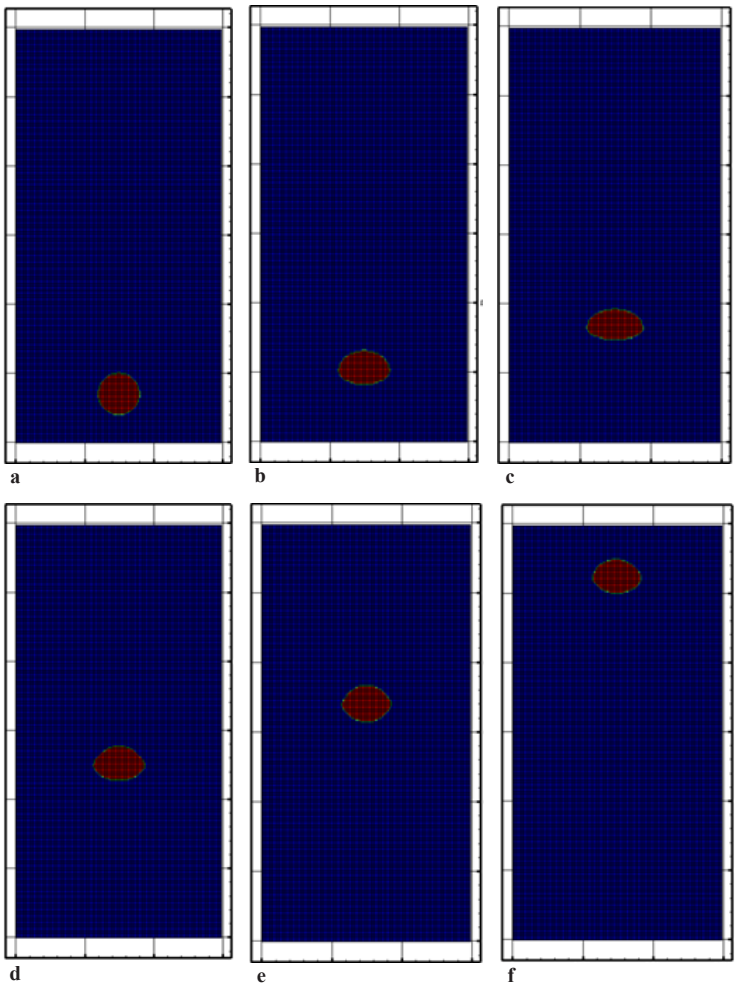

Figure 4. Profiles of the 2D contour enclosing the region where the gas volume fraction exceeds 0.5 at the following time instants: 0 (**a**), 23.3 (**b**), 47.3 (**c**), 77.9 (**d**), 115 (**e**), and 194 ms (**f**).

3D simulation of gas-bubble rise in liquid lead

The computational domain is a rectangular parallelepiped measuring 15 × 30 × 15 mm³ in XYZ space. The channel is filled with liquid lead with a density of 10^4 kg/m³ and is placed in a gravitational field (g = –10 m/s²). At the initial time, a spherical gas bubble of radius 1.5 mm and density 1 kg/m³ is located in the lower part of the channel (X_0 = 7.5 mm; Y_0 = 3.6 mm; Z_0=7.5 mm). The boundary conditions, equation-of-state parameters, initial thermodynamic values, and numerical settings are the same as those used in the preceding 2D simulation.

Fig. 5 shows the 3D results for the contour enclosing the region where the gas volume fraction exceeds 0.5 at the same time instants as in Fig. 4.

Fig. 6 presents the time histories of bubble-rise velocity for the 2D and 3D simulations, with output written every 40,000 computational steps. The rise velocity was calculated as the mass-averaged value within the contour corresponding to a gas volume fraction of 0.5. The same figure also includes dashed lines corresponding to experimental rise velocities for gas bubbles of different sizes in a 10 × 10 × 400 mm³ rectangular channel with a 3 mm inlet nozzle (Hibiki et al. 2000). The lower dashed line corresponds to the average rise velocity of small bubbles, the middle dashed line to medium-sized bubbles of nozzle scale, and the upper dashed line to large bubbles. The calculated rise velocity for a bubble with an initial diameter of 3 mm lies close to the middle dashed line, indicating good agreement with the experimental data.

Conclusions

The results of the 2D and 3D numerical simulations of a gas bubble rising in liquid lead, obtained using the previously developed surface-tension methodology integrated into the numerical algorithm of the two-phase flow code, are in good agreement with the experimental rise velocities reported for small bubbles. The observed discrepancy in the predicted bubble rise velocity, of the order of 40%, is mainly associated with the limited mesh resolution employed in the present calculations. One of the limitations of the current surface-tension formulation is its implementation on Cartesian grids, which constrains the geometrical flexibility of the numerical approach. Further studies will extend the analysis to a broader set of conditions, including variations in bubble rise velocity and channel geometry.

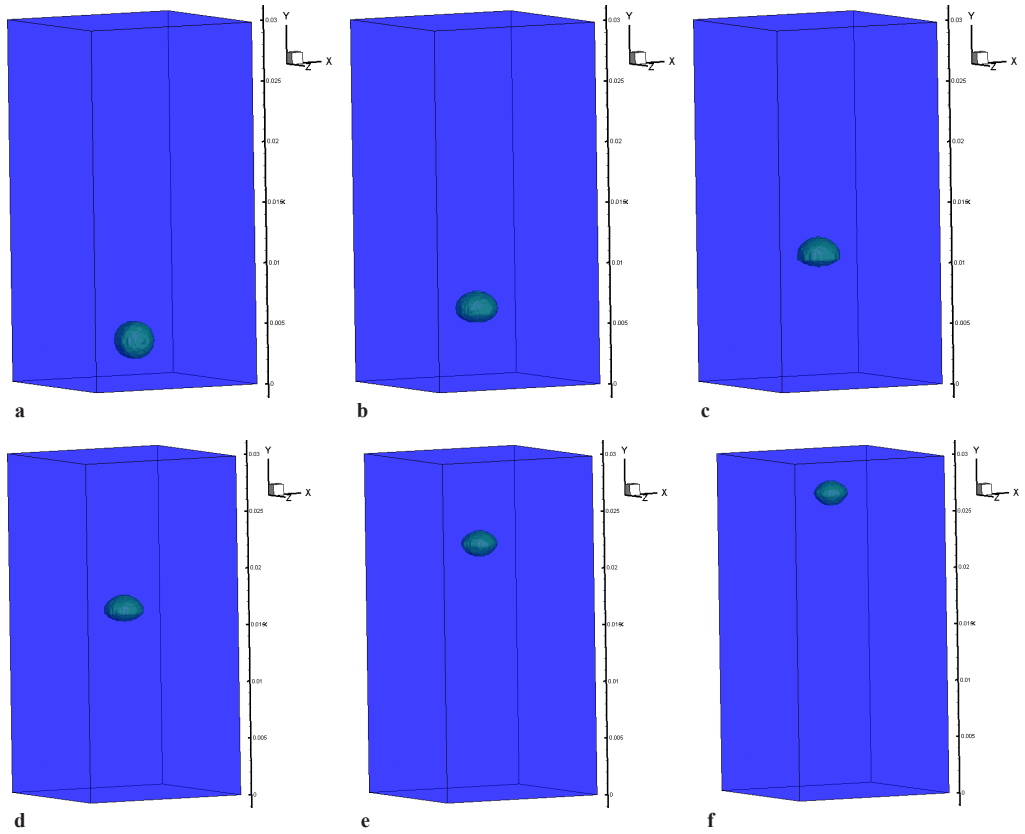

Figure 5. Profiles of the 3D contour enclosing the region where the gas volume fraction exceeds 0.5 at the following time instants: 0 (**a**), 23.3 (**b**), 47.3 (**c**), 77.9 (**d**), 115 (**e**), and 163 ms (**f**).

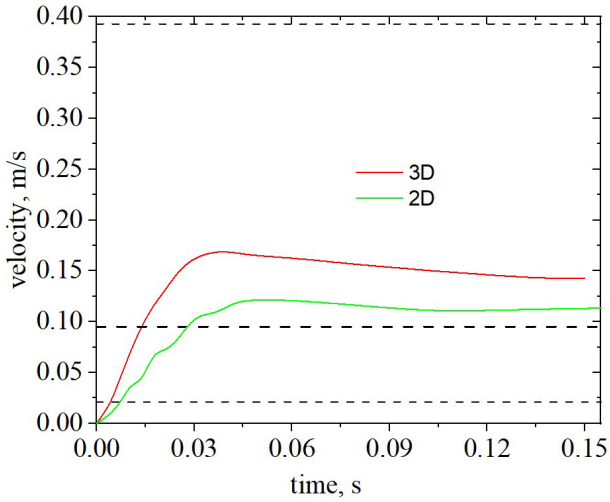

Figure 6. Time histories of bubble-rise velocity with output written every 40,000 computational steps for the 2D (green line) and 3D (red line) simulations; experimental rise velocities of bubbles (Hibiki et al. 2000) of various sizes (see text) shown by dashed lines.

References

- Berry RA, Saurel R, Petitpas F, Daniel E, Le Métayer O, Gavrilyuk S, Dovetta N, Martineau RC (2008) Progress in the development of compressible, multiphase flow modeling capability for nuclear reactor flow applications. INL Report, No. INL/EXT-08-15002, 143–168. https://doi.org/10.2172/946849
- Chudanov VV, Aksenova AE, Makarevich AA, Leonov AA (2025) 3D model of fluid surface tension in the TwoPhase code. Atomic Energy 138(6): 374–380. https://doi.org/10.1007/s10512-025-01269-x
- Hibiki T, Saito Y, Mishima K, Tobita Y, Konishi K, Matsubayashi M (2000) Study on flow characteristics in gas-molten metal mixture pool, Nuclear Engineering and Design 196: 223–245. https://doi.org/10.1016/S0029-5493(99)00293-9
- Khomyakov YS, Rachkov VI, Shvetsov IE (2023) Coupled modeling of neutronics and thermal-hydraulics processes in LFR under SG-leakage condition. Nuclear Energy and Technology 9(2): 85–92. https://doi.org/10.3897/nucet.9.99154

- Kuzina YuA, Sorokin AP (2024) Actual problems of modeling thermal-hydraulic processes in fast neutron reactors. Nuclear Energy and Technology 10(4): 241–250. https://doi.org/10.3897/nucet.10.139463
- Le Metayer O, Massoni J, Saurel R (2004) Elaborating equations of state of a liquid and its vapor for two-phase flow models. International Journal of Thermal Sciences 43: 265–276. https://doi.org/10.1016/j.ijthermalsci.2003.09.002
- Le Metayer O, Saurel R (2016) The noble-abel stiffened-gas equation of state. Physics of Fluids 28(4): 046102. https://doi.org/10.1063/1.4945981
- Lebaigue O, Duquennoy C, Vincent S (2004) Test-case number 1: Rise of a spherical cap bubble in a stagnant liquid (PN), Multiphase Science and Technology, Vol. 16, #1–3. https://doi.org/10.1615/MultScienTechn.v16.i1-3.20
- Pribaturin NA, Lobanov PD, Svetonosov AI, Kurdyumov AS, Chinak AV, Volkov SM (2024) Experimental study of gas bubble evolution in liquid metal. Thermophysics and Aeromechanics 31(3): 495–502. https://doi.org/10.1134/S0869864324030120
- Saurel R, Petiptas F, Berry RA (2009) Simple and efficient relaxation methods for interfaces separating compressible fluids, cavitating flows and shocks in multiphase mixtures. Journal of Computational Physics 228: 1678–1712. https://doi.org/10.1016/j.jcp.2008.11.002
- Toro EF (2019) The HLLC Riemann solver. Shock Waves 29: 1065–1082. https://doi.org/10.1007/s00193-019-00912-4
- Xiuzhong Sh, Takashi H (2021) Distribution parameter and drift velocity for upward gas-liquid metal two-phase flow. Applied Thermal Engineering 184:1–22. https://doi.org/10.1016/j.applthermaleng.2020.116242

Additional information

Conflict of interest
The authors have declared that no competing interests exist.

Ethical statement
No ethical statement was reported.

Artificial Intelligence (AI) Use
The authors accept full responsibility for the content of the manuscript, including the disclosure of any use of AI.
No AI tools were used in the preparation of this manuscript.

Funding
No funding was reported.

Author contributions
All authors have contributed equally.

Data availability
All of the data that support the findings of this study are available in the main text.